

# Ternary Rare Earth Inorganic–Organic Hybrids with a Mercapto-Functionalized Si–O Linkage and a Polymer Chain: Coordination Bonding Assembly and Luminescence

Kai Sheng,<sup>[a]</sup> Bing Yan,<sup>\*[a]</sup> Hai-Feng Lu,<sup>[a]</sup> and Lei Guo<sup>[a]</sup>

**Keywords:** Organic-inorganic hybrid composites / Rare earths / Polymers / Bridging ligands / Sulfur / Luminescence

A series of ternary organic/inorganic/polymer hybrid materials have been assembled on the basis of the coordination chemistry principle. Mercapto-functionalized MBA-Si from MBA (4-mercaptobenzoic acid) behaves as the first coordination unit, which forms sulfide linkages, resulting in an inorganic Si–O network after hydrolysis and copolycondensation with TEOS (tetraethoxysilane). The organic polymers PVPD [poly(4-vinylpyridine)] and PMMA [poly(methyl methacrylate)] play a role of the second coordination unit, whose or-

ganic polymeric C–C chain originates from addition polymerization of the monomers 4-VPD (4-vinylpyridine) and MMA (methyl methacrylate), respectively. These hybrids are characterized in detail to compare with the binary hybrids without an organic polymer unit, whose results reveal that the microstructure, the thermal stability, and especially the photoluminescence properties of the hybrid system are improved with the introduction of the polymer as the coligand.

## Introduction

The study on luminescent rare earth (especially  $\text{Eu}^{3+}$  and  $\text{Tb}^{3+}$ ) complexes has gained great interest during the past decades for their fascinating properties including high quantum efficiency, narrow emission bands, high color purity, large Stokes shifts, and long lifetime, which can be expected to have large potential applications in the fields of luminescent sensors, lasers, fluorescent probes, light-emitting diodes, optical amplifiers, and so on.<sup>[1]</sup> Nevertheless, due to their poor thermal stability and low mechanical resistances, rare earth complexes have been excluded from practical applications.<sup>[2]</sup> Therefore, many researchers incorporate rare earth complexes into an inert host (silica gel or polymer matrix) to construct organic–inorganic hybrids by using the sol–gel method<sup>[3,4]</sup> to combine remarkable mutual features of both organic and inorganic components.<sup>[5]</sup>

Typically, according to the interfacial force between the organic and inorganic phases of the hybrid materials, the synthetic procedures can be categorized into two main routes.<sup>[6]</sup> One is called the conventional doping method: the organic compound is dispersed or dissolved into an inorganic host through weak physical interactions (such as hydrogen bonding, van der Waals forces, or electrostatic forces)<sup>[7]</sup> and easily introduces inhomogeneity and leaching or clustering of the photoactive center, which results from

the high vibration energy of the hydroxy groups surrounding rare earth ions. The other synthesis method involving covalent bonds can avoid these shortcomings. The resulting hybrid materials show improved chemical stability and compatibility owing to the covalent linking of the two parts.<sup>[8]</sup> Thus, more and more attention has been paid to the chemically bonding method to construct organic–inorganic hybrid materials. Carlos et al. have done important work and have lately written a review on lanthanide-containing light-emitting organic–inorganic hybrids.<sup>[9]</sup> More recently, Binnemans gives a more extensive overview of the different types of lanthanide-based hybrid materials and compared their respective advantages and disadvantages.<sup>[10]</sup>

The critical step to assemble molecular-based hybrid materials is to design a functional molecular bridge that can coordinate rare earth ions and covalently bond to siloxanes.<sup>[11]</sup> Our group has realized six main modification paths, amino group, carboxyl group, hydroxy group, sulfonic group, and methylene group modification, and further introduced an organic polymer into the hybrid materials not only as a matrix but also as a component that can coordinate to the rare earth ions through the oxygen or nitrogen atom, as they have attractive properties such as low cost, light weight, easy to fabricate, and convenient to control various optical parameters.<sup>[12]</sup> In our organic/inorganic/polymer hybrid materials, the bridge molecule acts as small molecular ligand and the polymer acts as a macromolecular ligand or coligand.<sup>[13]</sup> Under these circumstances, both the small bridge molecules and the polymer can absorb excitation energy and transfer it to rare earth ions to obtain hybrid materials with excellent luminescent properties.

[a] Department of Chemistry, Tongji University, Siping Road 1239, Shanghai 200092, P. R. China  
Fax: +86-21-65982287  
E-mail: byan@tongji.edu.cn

Supporting information for this article is available on the WWW under <http://dx.doi.org/10.1002/ejic.201000273>.

In this paper, a mercapto-group-functionalized aromatic compound is selected for the preparation of the precursor, for the mercapto group is very active in many reactions.<sup>[14]</sup> Binary organic–inorganic hybrids based on 2-MBA (2-mercaptobenzoic acid) have been investigated in detail.<sup>[15]</sup> Here, we construct the ternary rare earth (Eu, Tb) organic/inorganic/polymeric hybrid materials based on 4-MBA by using a different polymer and the sol–gel method, and we synthesized the binary organic–inorganic hybrids simultaneously for comparison.

## Results and Discussion

The scheme for the synthesis process and the predicted compositions of the precursors and the binary and ternary hybrid materials are presented in Figure 1 and Figures S1 and S2 in the Supporting Information. As we know, it is very difficult to prove the exact structure of these kinds of noncrystalline hybrid materials, and it is hardly possible to solve the coordination behavior of rare earth ions. However, the main composition and their coordination effects can be predicted according to the rare earth coordination chemistry principle and the organic functional groups present. Considering the molecular structure of ligands 4-MBA-Si (P<sup>1</sup>, P<sup>2</sup>, P<sup>3</sup>), the carboxylate group remains after the mercapto modification of 4-MBA. So it can be assumed that the three COO<sup>−</sup> groups can provide six coordination sites from the chemical behavior of the aromatic carboxylates.<sup>[16]</sup> The S atom in the sulfide linkage is not coordinated to the rare earth ions because of its large steric hindrance and its weak coordination ability. For the ternary hybrids introduced by polymers PVPD [poly(4-vinylpyridine)] and PMMA [poly(methyl methacrylate)], the functional groups within them can provide one coordinated nitrogen atom (pyridine of PVPD) or oxygen atom (methacrylate of PMMA). Furthermore, according to the previous research of Horrocks,<sup>[17]</sup> it can be deduced that one or two water molecules may participate in the coordination of these hybrids. The prediction has also been confirmed by infrared spectra. Here it needs to be referred that the scheme is only to show the average coordination chemistry behavior around rare earth ions, which does not represent the exact structure of the hybrids.

The Fourier transform infrared spectra of the initial ligand MBA and the three precursors (P<sup>1</sup> denote MBA-TEPIC, P<sup>2</sup> denote MBA-APS and P<sup>3</sup> denote MBA-CPS, where TEPIC = 3-(triethoxysilyl)propyl isocyanate, APS = (3-aminopropyl)trimethoxysilane, and CPS = (3-chloropropyl)trimethoxysilane) are presented in Figure 2a. As is clearly seen, there exists a broad band centered at around 2934 and 2874 cm<sup>−1</sup> in the three precursors, which can be ascribed to the asymmetric stretching vibration and symmetric stretching vibration for the methylene (−CH<sub>2</sub>−) group of the coupling reagents. The vanishing of the ν(S−H) at 2541 cm<sup>−1</sup> for the three precursors compared to MBA and the appearance of the ν(C−S−C) at 696 cm<sup>−1</sup> suggest the modification of the coupling reagent. The large broad band

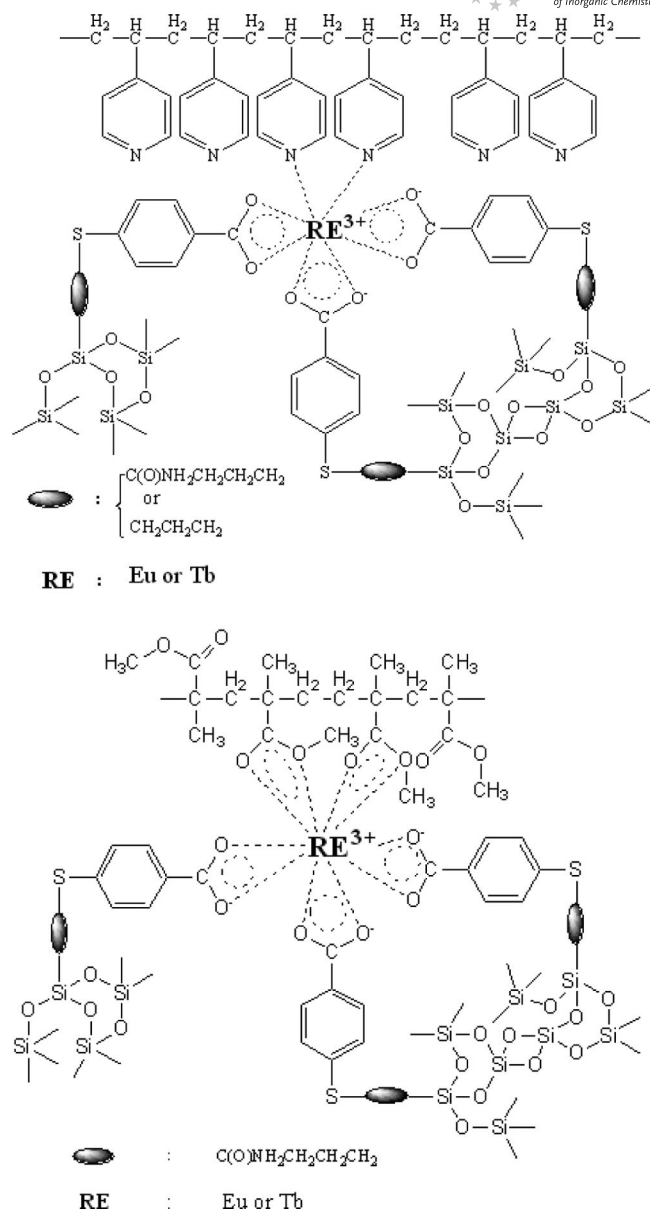


Figure 1. The predicted structure of the ternary hybrid materials.

at about 3414 cm<sup>−1</sup> and the low absorption peak at 921 cm<sup>−1</sup> in the three precursors are assigned to the stretching vibration and the out-of-plane bending vibration of O–H. The disappearance of the stretch vibration of (N=C=O) at 2250–2275 cm<sup>−1</sup> for P<sup>1</sup>, the ν(N–H) at 1209 cm<sup>−1</sup> for P<sup>2</sup>, and the ν(C–Cl) at 800 cm<sup>−1</sup> for P<sup>3</sup> indicate the coupling reagent is grafted onto MBA. Additionally, the existence of a stretching vibration of Si–C at 1196 cm<sup>−1</sup> and the stretching vibration of Si–O at 1099 and 1047 cm<sup>−1</sup> suggest the formation of the siloxane bonds. Figure 2b shows the FTIR spectra of selected hybrid materials. The two absorption bands at 1594 and 1424 cm<sup>−1</sup> correspond to the symmetric vibration and asymmetric vibration of the carbonyl group (COO<sup>−</sup>), respectively. The three absorption bands around 2934 cm<sup>−1</sup> are due to the −CH<sub>2</sub>− vibration, and the broad band at 3396 cm<sup>−1</sup> corresponds to the O–H (vs). The strong

peak at  $1383\text{ cm}^{-1}$  is assigned to the stretching vibration of  $\text{NO}_3^-$ , which indicates the nitrate group is not coordinated to  $\text{RE}^{3+}$ . Further, there also exists the Eu–O vibration at  $545\text{ cm}^{-1}$  which suggests the carbonyl group  $\text{COO}^-$  is coordinated to the rare earth ions. For PVPD-Eu- $\text{M}^1$ , the Eu–N vibration is located at  $476\text{ cm}^{-1}$ .

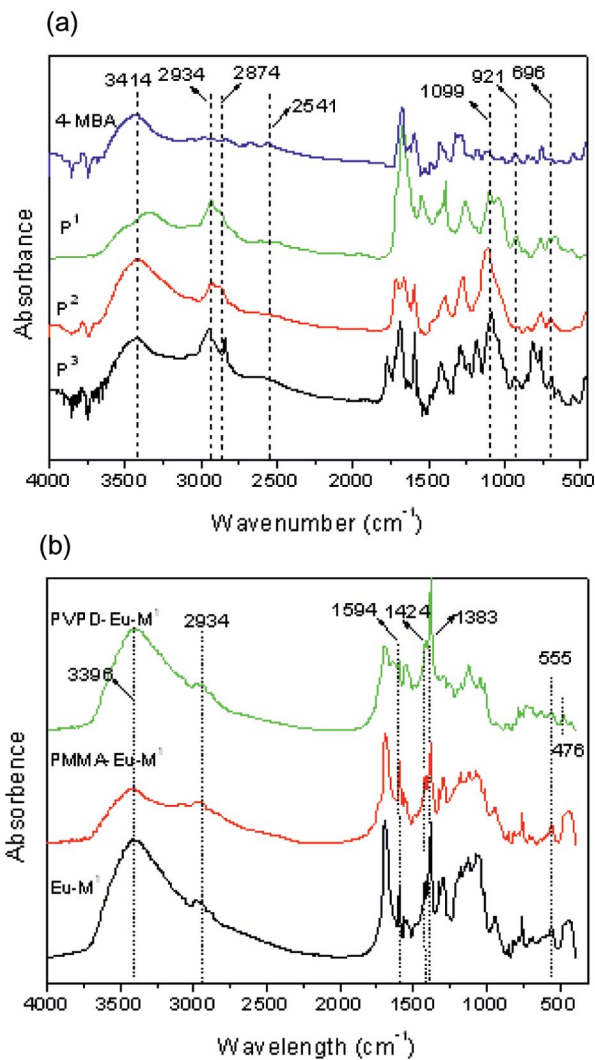


Figure 2. FTIR spectra of (a) the free ligand MBA and the three precursors MBA-Si ( $\text{P}^1$ ,  $\text{P}^2$ ,  $\text{P}^3$ , respectively) and (b) for the selected hybrids.

Figure 3 shows the ultraviolet absorption spectra ( $5 \times 10^{-4}\text{ M}$  DMF solution) of MBA,  $\text{P}^1$ ,  $\text{P}^2$ , and  $\text{P}^3$ . It is observed that there exists a broad absorption band for each compound (at 273, 264, 279, and 280 nm for MBA,  $\text{P}^1$ ,  $\text{P}^2$ , and  $\text{P}^3$ , respectively), which is ascribed to the major  $\pi$ – $\pi^*$  electronic transitions. Comparing the precursors with the original compound MBA, a blueshift (about 9 nm) of the absorption peak appears for  $\text{P}^1$ , whereas for  $\text{P}^2$  (about 6 nm) and  $\text{P}^3$  (about 7 nm) it shifted to a longer wavelength. This phenomenon indicates that the electron distribution of the conjugating system has changed after modification of MBA. Besides, we also can infer that the coupling reagents are grafted to MBA successfully.

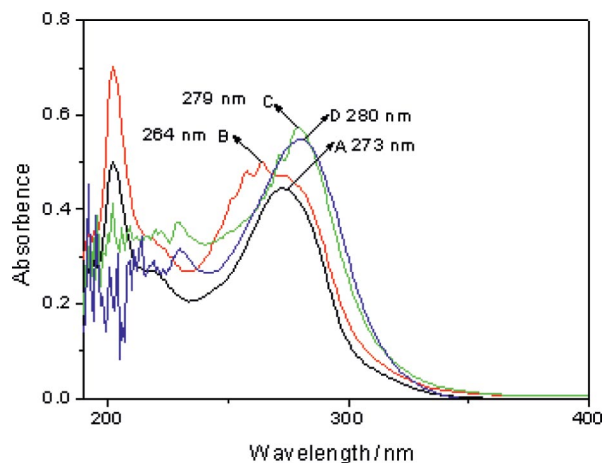


Figure 3. The ultraviolet absorption spectra of the free ligand MBA (A), precursors  $\text{P}^1$  (B), precursor  $\text{P}^2$  (C), and precursor  $\text{P}^3$  (D).

Figure S3 (Supporting Information) presents the X-ray diffraction (from  $10$  to  $70^\circ$ ) spectra of the selected hybrid materials Eu- $\text{M}^1$ , PVPD-Eu- $\text{M}^1$ , and PMMA-Eu- $\text{M}^1$ , which reveal that all the obtained hybrid materials are amorphous in the whole range. All the materials exhibit similar XRD patterns with a broad peak centered at around  $23^\circ$ , which is the characteristic diffraction of amorphous siliceous backbone material.<sup>[18]</sup> By comparison to the binary hybrids, there is no new diffraction peaks for the ternary hybrids with PVPD or PMMA, which show that the introduction of the macromolecular ligands in the hybrid system cannot affect the disordered silicon skeleton. Furthermore, there are many narrow weak peaks in these samples, corresponding to the incomplete hydrolysis–condensation of the excessive TEOS (tetraethoxysilane) molecules. TEOS molecules can carry on the hydrolysis–condensation process themselves or with a silane coupling reagent. If the hydrolysis–condensation process of the excessive TEOS molecules takes place among themselves, the ordered Si–O network can form a better crystal state. Then the narrow peaks appear, but the small amount of the ordered Si–O network brings the weak intensity. In addition, neither of the samples exhibit measurable amounts of the phase corresponding to the free ligands or the free salts, which can support the formation of the covalently bonded hybrids.

The DSC and TGA data for the ternary polymeric hybrid material PVPD-Eu- $\text{M}^1$  (Figure 4) shows 9% weight loss at  $170^\circ\text{C}$ , which is due to the loss of the residual and coordinated water molecule. Between  $170$  and  $600^\circ\text{C}$ , a weight loss of 37% is observed, which is ascribed to the decomposition of the organics in the material. Corresponding with this weight loss, are two obvious exothermic peaks at  $210$  and  $530^\circ\text{C}$  observed from the DSC curve, which is concordant with the pyrolysis of the material releasing energy. There are additional weight losses of 4% between  $600$  and  $800^\circ\text{C}$  and a very gradual loss of 1% at  $1000^\circ\text{C}$  without obvious absorbing and releasing energy in the DSC curve. The residual weight (49%) is mainly inorganic Si–O

networks ( $1090\text{ cm}^{-1}$  in FTIR). The results show that this kind of organic/inorganic/polymeric hybrid material is stable under  $210\text{ }^{\circ}\text{C}$ . This thermal stability is higher than the pure complex and also better than the binary organic/inorganic hybrid material according to the literature.<sup>[15]</sup>

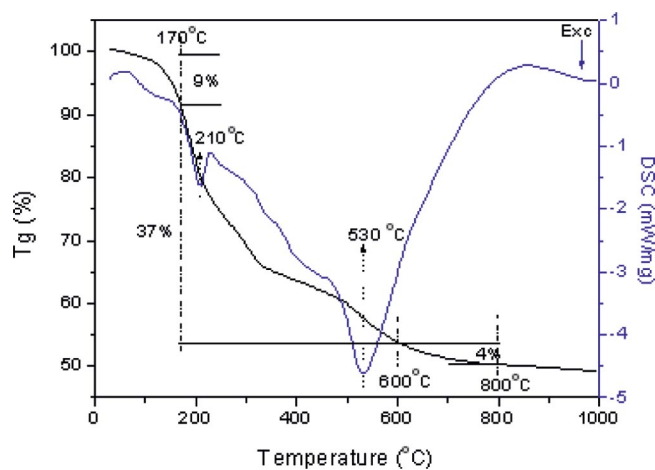


Figure 4. Selected DSC and TGA traces of the ternary hybrid material PVPD-Eu-M<sup>1</sup>.

Figure S4 (Supporting Information) and Figure 5 show the micrographs of the selected binary and ternary hybrid materials, respectively. It can be seen from the images of all hybrids that homogeneous systems are formed. Moreover, phase separation phenomenon cannot be observed, which always appears in the conventional doping method. By comparison with the binary and the ternary hybrid materials, we can observe distinct differences of the micro-morphology. For the binary hybrids, the microstructure exhibits the irregular shaped particles on the surface, whereas for the ternary hybrids, a more regular and uniform microstructure with ordered morphology on the surface can be obviously observed. This result verifies that the organic polymer (organic polymeric chains) may play an important role in the formation of the ultimate complicated hybrid system. For ternary hybrids, Figure 5a exhibits a petal-shaped, flake-layered, and globular structure. Figure 5b presents very ordered dendritic structure. Figure 5c,d show the perthitic structure with many small irregular particles on the surface. Figure 5e displays a regular and ordered globular structure. Figure 5f also has many ordered stripes with many small-sized uniform flake layers on the surface, which is amplified and clearly shown in Figure 5g for analysis. The luminescent center with the polymer is firstly accomplished by chelation not only through a small bridge molecule MBA-Si but also through macromolecular ligands PVPD or PMMA. Owing to the coordination effect and the steric hindrance of the polymer (as the terminal ligand), the structure of the luminescent center becomes rigid. Subsequently, the cohydrolysis and copolycondensation process is completed around the luminescent center. Therefore, it is easy to form a flake or globular structure. The flake structure can be stacked to petal shaped or layer shaped under different experimental conditions (polarity of the solvent,

for example). Moreover, the polymers PVPD or PMMA behave as the terminal ligand through simple chelation of the nitrogen or oxygen atom. The long organic chains supply the template effect to induce the cohydrolysis and copolycondensation process, which results in the long dendritic or stripe-shaped morphology. In summary, we can conclude that a more ordered and regular microstructure can be achieved with the introduction of the polymer.

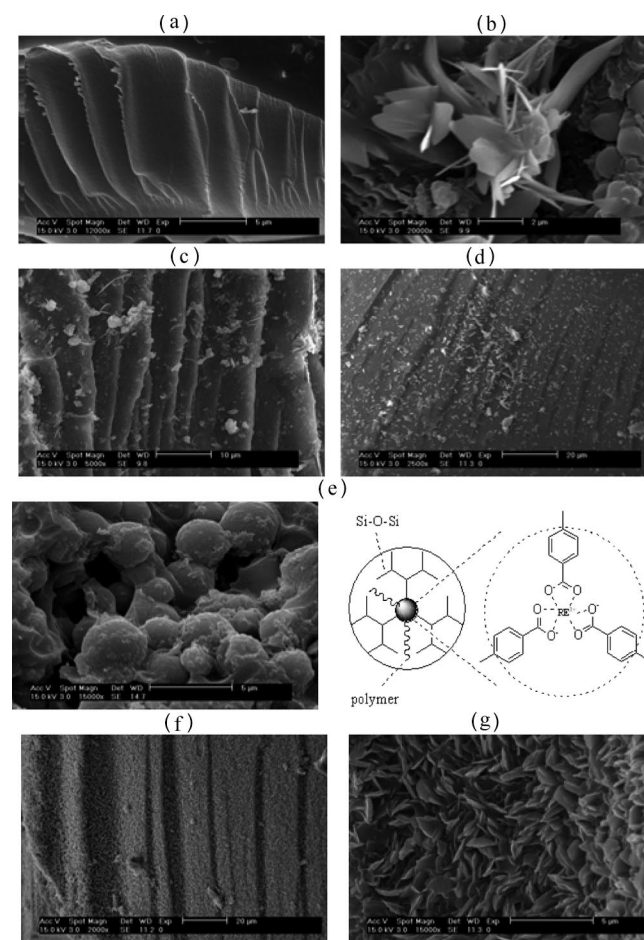


Figure 5. SEM images of the ternary hybrid materials: (a) PVPD-Eu-M<sup>1</sup>, (b) PMMA-Eu-M<sup>1</sup>, (c) PMMA-Eu-M<sup>2</sup>, (d) PVPD-Eu-M<sup>3</sup>, (e) PVPD-Tb-M<sup>1</sup>, (f) PMMA-Tb-M<sup>3</sup>, (g) amplified image of (f).

Figure S5 (Supporting Information) exhibits the UV/Vis diffuse reflection absorption spectra of selected europium and terbium hybrids. As can be seen, there is a large broad absorption band in each hybrid that is attributed to the  $\pi-\pi^*$  electronic transition of the aromatic ring in the hybrid system. It is worth noting that the large broad band overlaps from 220 to 500 nm, which proves that not only the small molecular ligand MBA could absorb abundant energy in the UV/Vis region, but the macromolecular ligand PVPD or PMMA can also enhance the absorbance ability. This energy can be transferred to rare earth ions through the “antenna effect” and sensitize the rare earth ions.

Figure 6 show the selected excitation spectra of all the europium hybrid materials in the solid state at room temperature, which are preformed under the maximum wave-

length of 613 nm for  $\text{Eu}^{3+}$ . A broad absorption band in the range from 220 to 450 nm is attributed to the mercapto-modified Si–O linkage host.<sup>[19]</sup> Here, the organically modified Si–O hybrid hosts not only behaves as the host but also as the ligands for the coordination bonds between MBA-Si ( $\text{M}^1$ ,  $\text{M}^2$ ,  $\text{M}^3$ ) and  $\text{Eu}^{3+}$ .<sup>[20]</sup> The absorption of the photoactive organically modified group and the –Si–O– network both play a role in the energy transfer and luminescence of  $\text{Eu}^{3+}$  within the hybrid systems. It is noteworthy that the wide excitation bands should contain the charge transfer state of Eu–O between  $\text{Eu}^{3+}$  and the MBA-Si unit. Besides, the weak narrow lines located at 393 nm are probably due to transitions within the  $4f^6$  configuration of  $\text{Eu}^{3+}$  ( ${}^7\text{F}_0 \rightarrow {}^5\text{L}_6$  transition) and overlapped with the wide excitation of the host.<sup>[21]</sup>

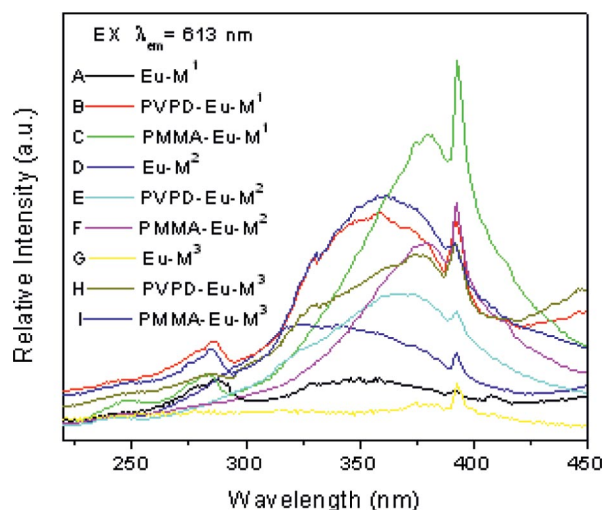


Figure 6. Selected excitation spectra of the europium hybrid materials; the curves from A to I denote Eu/Tb- $\text{M}^1$ , PVPD-Eu/Tb- $\text{M}^1$ , PMMA-Eu/Tb- $\text{M}^1$ , Eu/Tb- $\text{M}^2$ , PVPD-Eu/Tb- $\text{M}^2$ , PMMA-Eu/Tb- $\text{M}^2$ , Eu/Tb- $\text{M}^3$ , PVPD-Eu/Tb- $\text{M}^3$ , PMMA-Eu/Tb- $\text{M}^3$ , respectively.

Figure 7 presents the luminescence spectra of ternary europium and terbium organic/inorganic/polymeric hybrid materials in the visible range (from 550 to 700 nm for europium and from 400 to 600 nm for terbium). For europium hybrids, all the emission spectra display the characteristic  $\text{Eu}^{3+}$   ${}^5\text{D}_0 \rightarrow {}^7\text{F}_J$  ( $J = 0-4$ ) intra- $4f^6$  transitions at 575, 589, 614, 649, and 700 nm, respectively.<sup>[19]</sup> Among these emission peaks, the orange emission at 589 nm and the predominant red emission at 614 nm (associated with  ${}^5\text{D}_0 \rightarrow {}^7\text{F}_1$  and  ${}^5\text{D}_0 \rightarrow {}^7\text{F}_2$  transitions, respectively) are obviously observed, whereas the other transitions are relatively weaker. The detailed luminescence data are shown in Table 1. As we know, the  ${}^5\text{D}_0 \rightarrow {}^7\text{F}_2$  transition is the electric dipole transition with hypersensitivity to the local symmetry of the coordination sphere of the  $\text{Eu}^{3+}$  ions, whereas the magnetic dipole transition  ${}^5\text{D}_0 \rightarrow {}^7\text{F}_1$  is practically independent of the host material, so the intensity ratio of the red and orange intensities is considered as the coefficient to the symmetry around  $\text{Eu}^{3+}$ . When the ratio is higher, the europium ion generally occupies a lower symmetry microenvironment,<sup>[22]</sup> and the data shown in Table 1 indicate that the europium ion may oc-

cupy the low symmetry sphere in ternary hybrids containing PMMA. For terbium hybrids, we can see that the narrow emission lines are recorded upon a broad emission band from 350 to 650 nm. The narrow lines are ascribed to the characteristic  $\text{Tb}^{3+}$  emission with peaks at 486, 542, 581, and 618 nm corresponding to  ${}^5\text{D}_4 \rightarrow {}^7\text{F}_J$  ( $J = 6-3$ ), respectively, whereas the broad band are attributed to the emission of the organically modified Si–O group that is not transferred to the terbium ion.

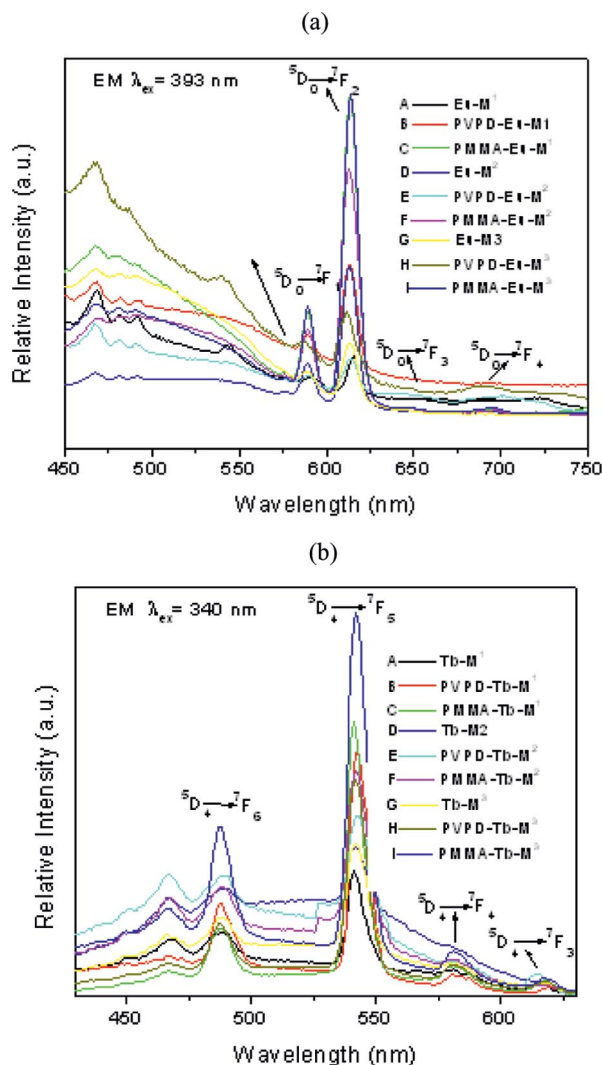


Figure 7. The emission spectra of (a) Eu hybrids and (b) Tb hybrids; the curves from B to J denote Eu/Tb- $\text{M}^1$ , PVPD-Eu/Tb- $\text{M}^1$ , PMMA-Eu/Tb- $\text{M}^1$ , Eu/Tb- $\text{M}^2$ , PVPD-Eu/Tb- $\text{M}^2$ , PMMA-Eu/Tb- $\text{M}^2$ , Eu/Tb- $\text{M}^3$ , PVPD-Eu/Tb- $\text{M}^3$ , PMMA-Eu/Tb- $\text{M}^3$ , respectively.

For further investigation of the photoluminescence properties, we measure the decay curves of all the europium and terbium hybrid materials at room temperature. All the typical decay curves can be described as a single exponential ( $\ln[S(t)/S_0] = -k_1t = -t/\tau$ ; Figure S6 in the Supporting Information shows the decay curve of the Eu- $\text{M}^1$  hybrids). The resulting luminescent lifetimes of the europium hybrids are summarized in Table 1. Furthermore, we selectively determined the emission quantum efficiency of the  ${}^5\text{D}_0$   $\text{Eu}^{3+}$  excited state for europium-containing hybrids on the basis of

Table 1. Luminescence efficiencies and lifetimes for the europium hybrid materials.

Hybrid Materials	$I_{02}/I_{01}$ <sup>[a]</sup>	$\tau$ [ms] <sup>[b]</sup>	$A_r$	$A_{nr}$	$\eta$ [%] <sup>[c]</sup>	$n_w$
Eu-M <sup>1</sup>	2.67	0.432	195	2120	8	~
PVPD-Eu-M <sup>1</sup>	3.77	0.485	224	1839	11	~2
PMMA-Eu-M <sup>1</sup>	3.65	1.052	241	951	25	~1
Eu-M <sup>2</sup>	2.21	0.478	176	1916	8	~2
PVPD-Eu-M <sup>2</sup>	3.49	0.618	228	1390	14	~1.5
PMMA-Eu-M <sup>2</sup>	3.52	0.794	229	1030	18	~1
Eu-M <sup>3</sup>	2.25	0.43	194	2132	8	~2
PVPD-Eu-M <sup>3</sup>	3.03	0.658	187	1333	12	~1.5
PMMA-Eu-M <sup>3</sup>	3.31	0.958	220	824	21	~1

[a] Integrated intensity of the  ${}^5D_0 \rightarrow {}^7F_J$  emission curves. [b] For the  ${}^5D_0$  excited state of  $Eu^{3+}$ , whose error is  $\pm 50 \mu s$ . [c] For  ${}^5D_0$  quantum efficiency.

emission spectra and the lifetimes of the  ${}^5D_0$  emitting level. Assuming that only nonradiative and radiative processes are essentially involved in the depopulation of the  ${}^5D_0$  state,  $\eta$  can be defined by Equation (1).<sup>[23]</sup>

$$\eta = \frac{A_r}{A_r + A_{nr}} \quad (1)$$

Here,  $A_r$  and  $A_{nr}$  represent radiative and nonradiative transition rates, respectively.  $A_r$  can be obtained by summing over the radiative rates  $A_{0J}$  for each  ${}^5D_0 \rightarrow {}^7F_J$  ( $J = 0-4$ ) transition of  $Eu^{3+}$ . Because  ${}^5D_0 \rightarrow {}^7F_1$  belongs to the isolated magnetic dipole transition, it is practically independent of the chemical environments around the  $Eu^{3+}$  ion as an internal reference for the whole spectra; the experimental coefficients of spontaneous emission,  $A_{0J}$ , can be calculated according to the equation.<sup>[24,25]</sup> The emission intensity,  $I$ , taken as integrated intensity  $S$  of the  ${}^5D_0 \rightarrow {}^7F_{0-4}$  emission curves. On the basis of the above discussion, the quantum efficiencies of the europium hybrid materials can be determined, as shown in Table 1. Seen from Equation (1), the value  $\eta$  mainly depends on the values of two factors: one is lifetime and the other is  $I_{02}/I_{01}$  (red/orange ratio). If the lifetime and red/orange ratio are large, the quantum efficiency must be high. As can be seen clearly from Table 1, the quantum efficiencies of the europium hybrid materials are determined in the order: PMMA-Eu-M > PVPD-Eu-M > PMAA-Eu-M for the same coupling reagent. That is, the ternary polymer-containing hybrids exhibit higher luminescence quantum efficiency than the binary hybrids, in particular, the ternary PMMA polymer-containing hybrids show the highest luminescence quantum efficiency, which are in accord with the order of luminescence intensities and lifetimes. The results reveal that with the introduction of the polymer as the macromolecule ligand or coligand, the luminescence properties of the overall hybrid system are improved by the increasing ratio of the radiative transitions. Here it is noteworthy that the absolute overall quantum yields had better be measured in order to show the real luminescent behavior, but here we merely want to compare the different hybrids relatively. The deep investigation needs to be underway.

To study the coordination environment surrounding the lanthanide ions, especially the influence caused by vibrations of water molecules according to Horrocks,<sup>[15]</sup> it is expected that the probable number of coordinated water molecules ( $n_w$ ) can be calculated by Equation (2).

$$n_w = 1.05 (A_{exp} - A_{rad}) \quad (2)$$

On the basis of the results, the coordination number of water molecules (Eu containing hybrid materials) can be estimated to be 1–2. The coordination water molecules produce severe vibrations of the hydroxy group, resulting in large nonradiative transitions and a decrease in the luminescent efficiency. The 4-MBA-Si (P<sup>1</sup>, P<sup>2</sup>, P<sup>3</sup>) bridge molecules provide three coordinated  $COO^-$  groups to occupy the equal six coordination number and the functional group of polymers show the one coordinated N (PCPD) or O (PMMA) atom. So the total coordination number for the Eu (Tb) ion in the ternary hybrids is 8–9, which corresponds to rare earth coordination chemistry behavior.

## Conclusions

In summary, on the basis of coordination chemistry, ternary rare earth/organic/inorganic/polymeric hybrid materials containing both inorganic networks (Si–O–Si, first ligand) and organic polymeric C–C chains (second ligand) have been assembled. The small bridge molecule ligand precursor MBA-Si is constructed through mercapto functionalization with different coupling reagents and the polymer ligand is synthesized by polymerization reaction. The results reveal that the ternary hybrid materials present more regular morphology, stronger luminescence intensity, longer lifetimes, and higher quantum efficiency than the binary hybrids, indicating that the introduction of the polymer can induce the self-assembly process of the microstructure and sensitize the luminescence of the hybrid materials.

## Experimental Section

**Materials:** 4-Mercaptobenzoic acid (4-MBA), tetraethoxysilane (TEOS), and the three cross-linking reagents [3-(triethoxysilyl)propyl isocyanate (TEPIC), (3-aminopropyl)trimethoxysilane (APS), (3-chloropropyl)trimethoxysilane (CPS)] were all analytical reagents. Other starting reagents were used as received. Europium and terbium nitrates were obtained by dissolving the corresponding oxides in concentrated nitric acid.

**Synthesis of Precursors and Polymers:** Three precursors and the polymer are prepared according to ref.<sup>[13]</sup> and depicted in Figure S1 (Supporting Information).

**Precursor 1 (P<sup>1</sup>). Modification by TEPIC:** 4-MBA (1 mmol) was first dissolved in refluxing anhydrous THF by stirring, and then TEPIC (1 mmol) was added to the solution dropwise. The whole mixture was heated at reflux at 80 °C for 3 h under an atmosphere of argon in a covered flask. After cooling, the solvent was removed under reduced pressure, and then the residue was washed with hexane ( $3 \times 20$  mL). P<sup>1</sup> was obtained as a yellow oil. Yield: 0.34 g, 85%.  $C_{17}H_{27}NO_6SSi$  (401.56): calcd. C 50.85, H 6.78, N 3.49; found C 50.53, H 6.87, N 3.56.  ${}^1H$  NMR (400 MHz,  $CDCl_3$ ):  $\delta =$

0.63 (t, 2-H,  $\text{CH}_2\text{Si}$ ), 1.25 (t, 9-H,  $\text{CH}_2\text{CH}_3$ ), 1.57 (m, 2-H,  $\text{CH}_2\text{CH}_2\text{CH}_2$ ), 3.20 (t, 2-H,  $\text{CH}_2\text{CH}_2\text{CH}_2$ ), 3.73 (q, 6-H,  $\text{CH}_2\text{CH}_3$ ), 7.35 (q, 1-H,  $-\text{C}_6\text{H}_4$ ), 7.42 (t, 1-H,  $\text{NH}$ ), 7.68 (d, 1-H,  $-\text{C}_6\text{H}_4$ ), 7.87 (q, 1-H,  $-\text{C}_6\text{H}_4$ ), 8.74 (d, 1-H,  $-\text{C}_6\text{H}_4$ ), 11.30 (s, 1-H,  $\text{OH}$ ) ppm.

**Precursor 2 (P<sup>2</sup>). Modification by APS:** 4-MBA (1 mmol) was first dissolved in refluxing pyridine by stirring, and then APS (1 mmol) was added to the solution dropwise. The whole mixture was heated at reflux at 100 °C for 8 h under an atmosphere of argon in a covered flask. After cooling, the solvent was removed under reduced pressure, and then the residue was washed with hexane ( $3 \times 20$  mL). P<sup>2</sup> was obtained as a yellow oil. Yield: 0.31 g, 87%.  $\text{C}_{16}\text{H}_{26}\text{O}_5\text{SSi}$  (358.53): calcd. C 53.60, H 7.31; found C 53.23, H 7.23. <sup>1</sup>H NMR (400 MHz,  $\text{CDCl}_3$ ):  $\delta$  = 0.66 (t, 2-H,  $\text{CH}_2\text{Si}$ ), 1.25 (t, 9-H,  $\text{CH}_2\text{CH}_3$ ) 1.71 (m, 2-H,  $\text{CH}_2\text{CH}_2\text{CH}_2$ ), 3.17 (t, 2-H,  $\text{CH}_2\text{CH}_2\text{CH}_2$ ), 3.54 (q, 6-H,  $\text{CH}_2\text{CH}_3$ ), 7.21 (q, 1-H,  $-\text{C}_6\text{H}_4$ ), 7.45 (d, 1-H,  $-\text{C}_6\text{H}_4$ ), 7.76 (q, 1-H,  $-\text{C}_6\text{H}_4$ ), 7.97 (d, 1-H,  $-\text{C}_6\text{H}_4$ ), 11.02 (s, 1-H,  $\text{OH}$ ) ppm.

**Precursor 3 (P<sup>3</sup>). Modification by CPS:** 4-MBA (1 mmol) was first dissolved in DMF by stirring, and then CPS (1 mmol) was added to the solution dropwise.  $\text{K}_2\text{CO}_3$  (0.01 g) was added as catalyst. The whole mixture was heated at reflux at 120 °C for 6 h under an atmosphere of argon in a covered flask. After filtration, the solvent was removed under reduced pressure, and then the residue was washed with hexane ( $3 \times 20$  mL). P<sup>3</sup> was obtained as a yellow oil. Yield: 0.26 g, 83%.  $\text{C}_{13}\text{H}_{20}\text{O}_5\text{SSi}$  (316.45): calcd. C 49.34, H 6.37; found C 49.57, H 6.53. <sup>1</sup>H NMR (400 MHz,  $\text{CDCl}_3$ ):  $\delta$  = 0.75 (t, 2-H,  $\text{CH}_2\text{Si}$ ), 1.89 (m, 2-H,  $\text{CH}_2\text{CH}_2\text{CH}_2$ ), 3.13 (t, 2-H,  $\text{CH}_2\text{CH}_2\text{CH}_2$ ), 3.61 (s, 9-H,  $\text{CH}_3$ ), 7.12 (q, 1-H,  $-\text{C}_6\text{H}_4$ ), 7.30 (d, 1-H,  $-\text{C}_6\text{H}_4$ ), 7.78 (q, 1-H,  $-\text{C}_6\text{H}_4$ ), 8.08 (d, 1-H,  $-\text{C}_6\text{H}_4$ ), 11.02 (s, 1-H,  $\text{OH}$ ) ppm.

**Synthesis of the Polymer PVPD (PMMA):** 4-Vinylpyridine (PVPD) [or methyl methacrylate (PMMA)] (1 mmol) was weighed and transferred into a separating funnel. It was then washed with 0.1 M sodium hydroxide solution to remove the inhibitor. After oscillating for 5 min and standing for 2 h, the water phase and upper oil phase were separated. The residual water was removed with anhydrous copper sulfate. After purification and reduced pressure distillation under a nitrogen atmosphere, the monomer was injected into a covered three mouth flask with azobisisobutyronitrile (AIBN) (or benzoyl peroxide, BPO) as an initiator. The mixture was dissolved in methanol [or blend-solvent (BS) of toluene and ethyl acetate] and maintained at 65 °C (or 70 °C) for 8 h (or 6 h) under flowing high-purity nitrogen. After removal of the solvent, a canary yellow and stringy liquid was obtained. The product was dried in a vacuum desiccator after recrystallization by using methanol and anhydrous ether (see Figure S1, Supporting Information).

**Synthesis of the Binary (Ternary) Rare Earth Inorganic/Organic/Polymeric Hybrid Materials:** The binary hybrids are prepared according to ref.<sup>[13]</sup> (Figure S2, Supporting Information). The typical procedure for the preparation of the ternary hybrid materials is as follows (Figure 1). The above-prepared precursor (1 mmol) was dissolved in dry ethanol with stirring, and then a stoichiometric amount of  $\text{Ln}(\text{NO}_3)_3 \cdot 6\text{H}_2\text{O}$  [corresponding amount of polymer (PVPD for example) with DMF solution] was added dropwise. After 3 h, TEOS and  $\text{H}_2\text{O}$  were added to the solution to allow a sol-gel process, and then one drop of diluted hydrochloric acid was added to promote hydrolysis. The molar ratio of  $\text{Ln}(\text{NO}_3)_3 \cdot 6\text{H}_2\text{O}/\text{P}^1/(\text{Polymer})/\text{TEOS}/\text{H}_2\text{O}$  was 1:3:(3):6:24. After hydrolysis, an appropriate amount of hexamethylenetetramine was added to adjust to pH 6–7. The mixture was agitated magnetically in a covered Teflon beaker to obtain a single phase, and then it was aged at 65 °C for gelation in about 7 d. The final hybrid material named Eu-M<sup>1</sup> or Tb-M<sup>1</sup> (PVPD-Eu-M<sup>1</sup> or PVPD-Tb-M<sup>1</sup>) was collected as mono-

lithic bulks and ground into powdered material for the photophysical studies.

**Physical Measurements:** All measurements were performed at room temperature. Infrared spectra were recorded with a Nexus 912 AO439 FTIR spectrophotometer. We mixed the compound with the dried potassium bromide (KBr) and then pressed into pellets. The spectra were collected over the range 4000–400  $\text{cm}^{-1}$  by averaging 32 scans at a maximum resolution of 8  $\text{cm}^{-1}$ . <sup>1</sup>H NMR spectra were recorded in  $\text{CDCl}_3$  with a Bruker Avance-400 spectrometer with tetramethylsilane (TMS) as an internal reference. The ultraviolet absorption spectra ( $5 \times 10^{-4}$  M DMF solution) were recorded with an Agilent 8453 spectrophotometer. The UV/Vis diffuse reflection spectra of the powder samples were recorded with a BWS003 spectrophotometer. X-ray powder diffraction patterns were recorded by using a Rigaku D/max-rB diffractometer system equipped with a Cu anode in a  $2\theta$  range from 10 to 70°. Thermogravimetric analysis (TGA) and differential scanning calorimetry (DSC) traces were performed with a Netzsch STA 409 at a heating rate of 15 °C/min under a nitrogen atmosphere. The fluorescence spectra were obtained with a RF-5301 spectrophotometer equipped with a stablespec-xenon lamp (450 W) as the light source. Luminescent lifetimes were recorded with an Edinburgh FLS 920 phosphorimeter by using a 450-W xenon lamp as the excitation source (pulse width, 3  $\mu\text{s}$ ). The microstructures were checked by scanning electronic microscopy (SEM, Philips XL-30).

**Supporting Information** (see footnote on the first page of this article): Figures of the synthesis process of precursors or polymer, the binary hybrids, selected X-ray diffraction graph of hybrid materials, SEM of binary hybrids, UV/Vis diffuse reflection absorption spectra, and the decay curves of the hybrid materials.

## Acknowledgments

This work is supported by the National Natural Science Foundation of China (20971100) and the Program for New Century Excellent Talents in University (NCET-08-0398).

- [1] D. Parker, P. Kanthi-Senanayake, J. A. G. Williams, *J. Chem. Soc. Perkin Trans. 2* **1998**, 2129–2139; R. J. Curry, W. P. Gillin, *Curr. Opin. Solid State Mater. Sci.* **2001**, 5, 481–486; Y. X. Zheng, J. Lin, Y. J. Liang, Q. Lin, Y. N. Yu, Q. G. Meng, Y. H. Zhou, S. B. Wang, H. Y. Wang, H. J. Zhang, *J. Mater. Chem.* **2001**, 11, 2615–2619; J. C. G. Bünzli, C. Piguet, *Chem. Rev.* **2002**, 102, 1897–1928; J. Kido, Y. Okamoto, *Chem. Rev.* **2002**, 102, 2357–2368; T. Oyamada, Y. Kawamura, T. Koyama, H. Sasabe, C. Adachi, *Adv. Mater.* **2004**, 16, 1082–1086; C. M. G. dos Santos, P. B. Fernandez, S. E. Plush, J. P. Leonard, T. Gunnlaugsson, *Chem. Commun.* **2007**, 32, 3389–3391.
- [2] L. R. Matthews, E. T. Kobbé, *Chem. Mater.* **1993**, 5, 1697–1700.
- [3] Q. M. Wang, B. Yan, *J. Mater. Chem.* **2004**, 14, 2450–2454; Q. M. Wang, B. Yan, *Cryst. Growth Des.* **2006**, 5, 497–503; Q. M. Wang, B. Yan, *J. Photochem. Photobiol. A: Chem.* **2006**, 177, 1–6; B. Yan, Q. M. Wang, *J. Photochem. Photobiol. A: Chem.* **2008**, 197, 213–219; J. L. Liu, B. Yan, *J. Phys. Chem. B* **2008**, 112, 10898–10907; Y. Li, B. Yan, H. Yang, *J. Phys. Chem. C* **2008**, 112, 3959–3968; B. Yan, Q. M. Wang, *Cryst. Growth Des.* **2008**, 6, 1484–1489; H. F. Lu, B. Yan, J. L. Liu, *Inorg. Chem.* **2009**, 48, 3966–3975.
- [4] L. H. Wang, W. Wang, W. G. Zhang, E. T. Kang, W. Huang, *Chem. Mater.* **2002**, 12, 2212–2218; P. Lenaerts, A. Storms, J. Mullens, J. Dhaen, C. Görller-Walrand, K. Binnemans, K. Driesen, *Chem. Mater.* **2005**, 17, 5194–5201; S. Moynihan, R. Van Deun, K. Binnemans, J. Krueger, G. von Papen, A. Kew-

- ell, G. Crean, G. Redmond, *Optical Mater.* **2007**, *29*, 1798–1808; B. Yan, X. F. Qiao, *J. Phys. Chem. B* **2007**, *111*, 12362–12374.
- [5] A. C. Franville, D. Zambon, R. Mahiou, S. Chou, Y. Troin, J. C. Cousseins, *J. Alloys Compd.* **1998**, *275–277*, 831–834; S. Capecci, O. Renault, D. G. Mon, M. Halim, M. Etchells, R. J. Dobson, O. V. Salata, V. Christou, *Adv. Mater.* **2000**, *12*, 1591–1594.
- [6] C. Sanchez, F. Ribot, *New J. Chem.* **1994**, *18*, 1007–1037.
- [7] L. D. Carlos, R. A. S. Ferreira, J. P. Rainho, V. D. Bermudez, *Adv. Funct. Mater.* **2002**, *12*, 819–823; L. N. Sun, H. J. Zhang, L. S. Fu, F. Y. Liu, Q. G. Meng, C. Y. Peng, J. B. Yu, *Adv. Funct. Mater.* **2005**, *15*, 1041–1048; P. P. Lima, R. A. S. Ferreira, R. O. Freire, P. F. A. Almeida, L. S. Fu, J. S. Alves, L. D. Carlos, O. L. Malta, *ChemPhysChem* **2006**, *7*, 735–746.
- [8] A. C. Franville, R. Mahiou, Y. Troin, D. Zambon, J. C. Cousseins, *Solid State Sci.* **2001**, *3*, 211–222; P. N. Minoofar, R. Hernandez, S. Chia, B. Dunn, J. I. Zink, A. C. Franville, *J. Am. Chem. Soc.* **2002**, *124*, 14388–14396; J. Choi, R. Tamaki, S. G. Kim, R. M. Laine, *Chem. Mater.* **2003**, *15*, 3365–3375; J. H. Harreld, A. Esaki, G. D. Stucky, *Chem. Mater.* **2003**, *15*, 3481–3489.
- [9] L. D. Carlos, R. A. S. Ferreira, V. D. Bermudez, J. L. S. Ribeiro, *Adv. Mater.* **2009**, *21*, 509–534.
- [10] K. Binnemans, *Chem. Rev.* **2009**, *109*, 4283–4374.
- [11] V. D. Bermudez, L. D. Carlos, M. C. Duarte, M. M. Silva, C. J. Silva, M. J. Smith, M. Assuncao, L. Alcacer, *J. Alloys Compd.* **1998**, *275*, 21–26; A. C. Franville, D. Zambon, R. Mahiou, S. Chou, Y. Troin, J. C. Cousseins, *J. Alloys Compd.* **1998**, *275–277*, 831–834; L. D. Carlos, V. D. Bermudez, R. A. S. Ferreira, *J. Non-Cryst. Solids* **1999**, *247*, 203–208; H. R. Li, J. Lin, H. J. Zhang, H. C. Li, L. S. Fu, Q. G. Meng, *Chem. Commun.* **2001**, 1212–1213; X. M. Guo, H. D. Guo, L. S. Fu, H. J. Zhang, L. D. Carlos, R. P. Deng, J. B. Yu, *J. Photochem. Photobiol. A: Chem.* **2008**, *200*, 318–324.
- [12] M. I. Sarwar, Z. Ahmad, *Eur. Polym. J.* **2000**, *36*, 89–94; D. Liu, Z. G. Wang, *Polymer* **2008**, *49*, 4960–4967.
- [13] N. Sabbatini, M. Guardigli, J. M. Lehn, *Coord. Chem. Rev.* **1993**, *123*, 201–208; J. Erostyak, A. Buzady, A. Kaszas, J. Kozma, I. Hornyak, *J. Lumin.* **1997**, *72*, 570–574; A. Beeby, S. Faulkner, *Chem. Phys. Lett.* **1997**, *266*, 116–122; V. Bekiari, P. Lianos, *Adv. Mater.* **1998**, *10*, 1455–1458; K. Driesen, R. V. Deun, C. Görrler-Walrand, K. Binnemans, *Chem. Mater.* **2004**, *16*, 1531–1535.
- [14] L. N. Nikolenko, V. A. Koptug, *Zh. Obshch. Khim.* **1955**, *25*, 1757–1760; M. Bandini, P. G. Cozzi, M. Giacomini, P. Melchiorre, S. Selva, A. Umani-Ronchi, *J. Org. Chem.* **2002**, *67*, 3700–3704; G. Tarzia, A. Duranti, A. Tontini, *J. Med. Chem.* **2003**, *39*, 2352–2360; S. Vijaikumar, K. Pitchumani, *J. Mol. Catal. A* **2004**, *217*, 117–120; F. Fringuelli, F. Pizzo, C. Vittorini, L. Vaccaro, *Eur. J. Org. Chem.* **2006**, *5*, 1231–1236.
- [15] B. Yan, H. F. Lu, *Inorg. Chem.* **2008**, *47*, 5601–5611; B. Yan, K. Qian, *J. Organomet. Chem.* **2009**, *694*, 3160–3166.
- [16] J. F. Ma, J. Z. Ni, *Prog. Chem.* **1996**, *8*, 264.
- [17] W. De W. Horrocks Jr., D. R. Sudnick, *J. Am. Chem. Soc.* **1979**, *101*, 334–340; W. De W. Horrocks Jr., D. R. Sudnick, *Acc. Chem. Res.* **1981**, *14*, 384–392.
- [18] L. D. Carlos, V. D. Bermudez, R. A. S. Ferreira, L. Marques, M. Assuncao, *Chem. Mater.* **1999**, *11*, 581–588; H. S. Hoffmann, P. B. Staudt, T. M. H. Costa, C. C. Moro, E. V. Benvenuti, *Surf. Interface Anal.* **2002**, *33*, 631–634; M. C. Goncalves, V. D. Bermudez, R. A. S. Ferreira, L. D. Carlos, D. J. Ostrovskii, J. Rocha, *Chem. Mater.* **2004**, *16*, 2530–2543.
- [19] M. D. Regulacio, M. H. Publico, J. A. Vasquez, P. N. Myers, S. Gentry, M. Prushan, S. W. Tam-Changand, S. L. Stoll, *Inorg. Chem.* **2008**, *47*, 1512.
- [20] M. Kawa, J. M. J. Fréchet, *Chem. Mater.* **1998**, *10*, 286–296.
- [21] C. Y. Peng, H. J. Zhang, J. B. Yu, Q. G. Meng, L. S. Fu, H. R. Li, L. N. Sun, X. M. Guo, *J. Phys. Chem. B* **2005**, *109*, 15278–15287.
- [22] A. F. Kirby, D. Foster, F. S. Richardson, *Chem. Phys. Lett.* **1983**, *95*, 507–512.
- [23] R. A. S. Ferreira, L. D. Carlos, R. R. Gonçalves, S. J. L. Ribeiro, V. D. Bermudez, *Chem. Mater.* **2001**, *13*, 2991–2998; P. C. R. Soares-Santos, H. I. S. Nogueira, V. Félix, M. G. B. Drew, R. A. S. Ferreira, L. D. Carlos, T. Trindade, *Chem. Mater.* **2003**, *15*, 100–108.
- [24] M. H. V. Werts, R. T. F. Jukes, J. W. Verhoeven, *Phys. Chem. Chem. Phys.* **2002**, *4*, 1542–1548.
- [25] J. C. Boyer, F. Vetrone, J. A. Capobianco, A. Speghini, M. Bettinelli, *J. Phys. Chem. B* **2004**, *108*, 20137–20144.

Received: March 10, 2010

Published Online: June 21, 2010